EXOTICS SEARCHES IN ATLAS*

Michiru Kaneda

on behalf of the ATLAS Collaboration

CERN, 1211 Geneva 23, Switzerland

(Received April 30, 2013)

Beyond Standard Model scenarios are being searched for signatures with the ATLAS detector, which is placed on the one of interaction points of the Large Hadron Collider. More than 40 results based on 7 TeV data collected in 2011 were published or submitted to papers. There are already available six publications based on 8 TeV data collected in 2012. No indications for New Physics have been found, and limits on many theories are presented in a few hundreds GeV to a few TeV scale. In this presentation, recent results of such new physics searches are presented.

DOI:10.5506/APhysPolB.44.1495
PACS numbers: 12.60.–i, 13.85.–t

1. Introduction

The Standard Model (SM) of particle physics has made significant successes for the last few decades. On the other hand, the SM still has some unsolved problems, such as the hierarchy problem between forces or the origin of the Dark Matter. Several Beyond Standard Model theories are being studied to solve problems in the SM. Some of these theories expect New Physics at TeV scale, accessible at the Large Hadron Collider (LHC) [1]. Supersymmetry (SUSY) [2–4] is one of the candidates for the Beyond Standard Model (BSM). In addition, there are many "Exotics" physics scenarios and several phenomena are expected at the LHC.

The LHC started TeV scale proton–proton collisions (pp) in 2010. It provided pp collisions at the center-of-mass energy, $\sqrt{s}$, equal to 7 TeV in 2010 and 2011, and 8 TeV pp collisions in 2012. The ATLAS detector [5] is one of the general-purpose detectors at the LHC. Searches for New Physics are performed with the data collected by the ATLAS detector. This paper introduces recent results of these New Physics searches.

* Presented at the Cracow Epiphany Conference on the Physics After the First Phase of the LHC, Kraków, Poland, January 7–9, 2013.

2. New phenomena in dijet mass

A search for new phenomena in dijet final states is reported in Ref. [6]. The analysis selects events with two high transverse momentum (p_{T}) jets and studies the invariant mass of the dijet (m_{jj}). The dijet invariant mass distribution is expected to be smooth. The background estimation is done by fitting the following function to the data

$$f(x) = p_1 (1-x)^{p_2} x^{p_3 + p_4 \ln x}, \tag{1}$$

where $x = m_{jj}/\sqrt{s}$. The dominant uncertainty comes from the jet energy scale uncertainty, which is as low as 4%, depending on p_{T} and pseudorapidity (η) of the jets[1].

The study is performed with 13 fb^{-1} of 8 TeV pp collision data. The maximum jet p_{T} is 2.34 TeV and the highest invariant mass is 4.69 TeV. Figure 1 (left) shows the reconstructed dijet mass distribution. The data distribution (filled points) is shown with the fitted function. The significance in number of the Gaussian standard deviation based on the Poisson distributions is also shown in the lower panel. The statistical test is performed on this distribution and shows that χ^2/NDF (number of degrees of freedom) is 15.5/18, which corresponds to a p-value of 0.61, indicating good agreement between data and the fitted function. Further study is performed with the BumpHunter [7] to establish the presence or absence of a localized resonance, and taking proper account of the "look elsewhere effect" [8]. No significance excess has been found in the analysed dataset.

As no significant deviation from the background prediction is found, 95% confidence level (C.L.) upper limits on the cross section times acceptance ($\sigma \times \mathcal{A}$) are set for a hypothetical narrow new particle decaying into a dijet. Figure 1 (right) shows the obtained limit on excited quark (q^*) production. The observed lower limit on the mass of q^* is 3.84 TeV.

The model independent results are shown in figure 2. Results are obtained by using the simplified Gaussian models. Three different mass width models are shown.

Since the ATLAS dijet mass resolution is about 5%, New Physics models with a width smaller than 7% should be compared to the result of 7% resolution model.

[1] At the ATLAS detector, the polar angle θ is defined as an angle from the beam axis and the azimuthal angle ϕ is the angle around the beam axis. The pseudo-rapidity, η, is defined as follows

$$\eta \equiv -\ln \tan\left(\frac{\theta}{2}\right). \tag{2}$$

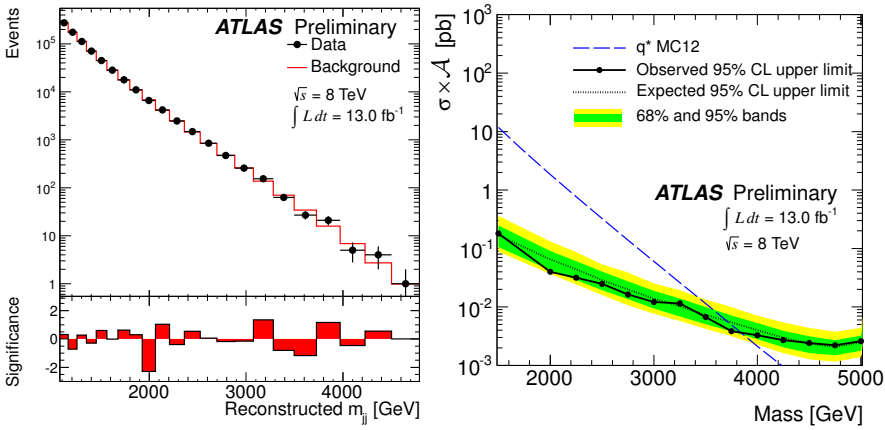

Fig. 1. Left: The reconstructed dijet mass distribution with statistical uncertainties (filled points with error bars) fitted with a smooth functional form (solid line). Right: The 95% C.L. upper limit on $\sigma \times \mathcal{A}$ as a function of dijet resonance mass. The dashed curve presents the excited-quark $\sigma \times \mathcal{A}$ prediction [6].

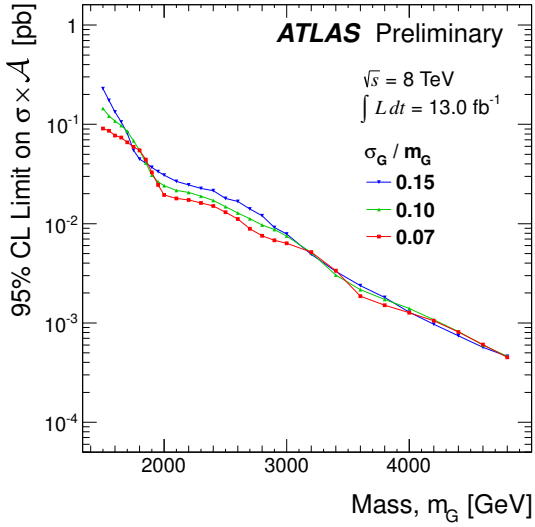

Fig. 2. The 95% C.L. upper limits on $\sigma \times \mathcal{A}$ for a simple Gaussian resonance [6].

3. High-mass dilepton resonances search

One of BSM, which introduces additional U(1)$'$ gauge symmetries, is associated with new heavy neutral gauge boson, called Z', as a result of the symmetry breaking of U(1)$'$ [10]. Such Z' is searched for in the dilepton

final states [11]. The Sequential Standard Model (SSM) [10] is used as the benchmark model of Z' (Z'_{SSM}) in present analysis, which uses 8 TeV pp collision data corresponding to an integrated luminosity of 6.1 fb^{-1}. The event selection requires two electrons or two muons. Muons are required to have at least three hits in each different plane of the outer muon system of the ATLAS detector to obtain optimal momentum resolution. This requirement results in low acceptance of 39% for Z'_{SSM} signal of 2 TeV mass in the muon channel, while the electron channel shows the acceptance of 70%.

The main background for both electron and muon channels is the Drell–Yan Z/γ^* process. The second largest background in the electron channel is QCD multijet. Other backgrounds are $t\bar{t}$, W+jets, and diboson production. In the muon channel, other backgrounds are $t\bar{t}$ and diboson productions. QCD multijet and W+jets processes are negligible in the muon channel.

Background estimation is based on the Monte Carlo simulation for all backgrounds except QCD multijet. For QCD multijet in the electron channel, the invariant mass distribution of dielectron (m_{ee}) is estimated from the control data distribution, which is obtained by "reverted electron identification" [12]. The invariant mass distribution in $80 < m_{ee} < 200$ GeV range of the control sample is fitted with QCD multijet and other backgrounds Monte Carlo samples to determine QCD multijet distribution. For higher mass region, the obtained QCD multijet distribution is fitted and extrapolated up to 500 GeV.

The total background is scaled to the data in the dilepton invariant mass (m_{ll}) range $80 < m_{ll} < 110$ GeV by fixing QCD multijet distribution. This has an advantage to cancel the luminosity uncertainty and other mass-independent uncertainties. The remaining mass-independent uncertainty is 5% from Z/γ^* cross section uncertainty.

One of the largest mass-depend uncertainties is the physics modeling uncertainty. It is 20% at $m_{ll} = 2$ TeV. For the electron channel, an uncertainty of QCD multijet estimation from the fit and an uncertainty of W+jet process from cross section are also large. They are about 21% in total.

Final dielectron invariant mass and dimuon invariant mass distributions after all selections are shown in figures 3 (a) and 3 (b), respectively. The data shows good agreement with the Standard Model expectation.

Figure 4 shows 95% exclusion limits on cross section (σ) times branching fraction (B) for the combined result of the electron and the muon channels.

The observed lower mass limit of 2.49 TeV is obtained for Z'_{SSM}, while the expected limit is 2.49 TeV. For gauge group E_6 motivated models [12], 2.09–2.24 TeV lower mass limits are obtained for each variation of the model.

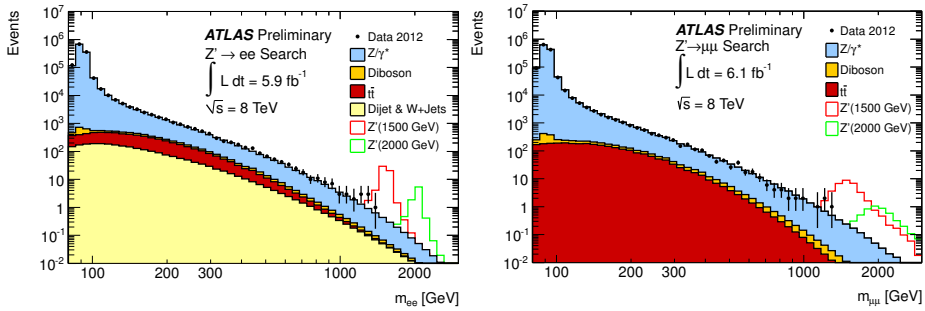

(a) (b)

Fig. 3. Figures (a) and (b) show dielectron invariant mass (m_{ee}) and dimuon invariant mass ($m_{\mu\mu}$) distributions with statistical uncertainties after final selection, respectively. Two signal points of Z'_{SSM} are shown with the stacked sum of all expected backgrounds [11].

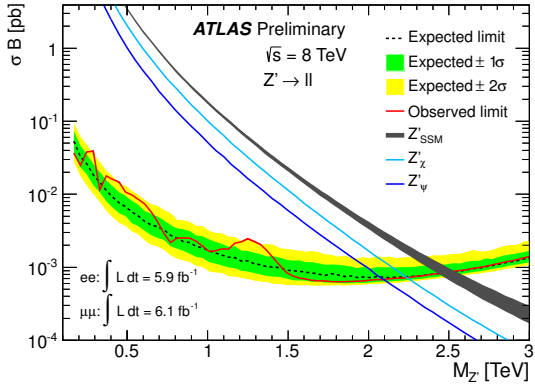

Fig. 4. Median expected (dashed line) and observed (solid line) 95% C.L. limits on $\sigma \times B$, and expected for $\sigma \times B$ for Z'_{SSM} and other two E_6-motivated Z' models for the combined result of the electron and the muon channels [11].

4. Resonant ZZ production search

The resonant search in $ZZ \to llqq$ final states ($l = e, \mu$) in pp collision at 8 TeV with an integrated luminosity of 7.2 fb^{-1} is presented in [14]. One of the candidates to make such a resonance is the spin-2 Randall–Sundrum Graviton (G^*) in the bulk RS1 [15]. In this model, the production and the decay of the G^* via light fermions are highly suppressed relative to RS1 [16], with strongly enhanced branching fractions of G^* to pairs of top quarks, W, Z, and Higgs bosons.

The event selection starts from selecting dijet and two electrons or two muons. The dilepton invariant mass is required to be in the Z boson mass range of $66 < m_{ll} < 116$ GeV.

In the higher ZZ mass region, a decayed Z boson is highly boosted. As a result, two quarks decayed from Z boson fall in the same jet, which is reconstructed with distance parameter of $\Delta R = 0.4$ [2]. Therefore, the analysis divides the events into the "resolved" region for low mass and the "merged" region for high mass, at ZZ mass of 1000 GeV. In the resolved region, two jets events are selected and the invariant mass of dijet is required to be in $65 < m_{jj} < 115$ GeV range. The azimuthal opening angle between two highest p_{T} jets is required to be less than 1.6. In addition, it is required that p_{T} of Z boson reconstructed from dilepton (p_{T}^{ll}) is greater than 50 GeV. ZZ mass is reconstructed from dijet and dilepton (m_{lljj}). The merged region requires the leading jet with $p_{\mathrm{T}} > 200$ GeV, mass of the leading jet (m_j) > 40 GeV, and $p_{\mathrm{T}}^{ll} > 200$ GeV. ZZ mass is reconstructed from the leading jet and dilepton (m_{llj}). The acceptance of signal events as a function of ZZ mass for both the resolved and merged regions are shown in figure 5.

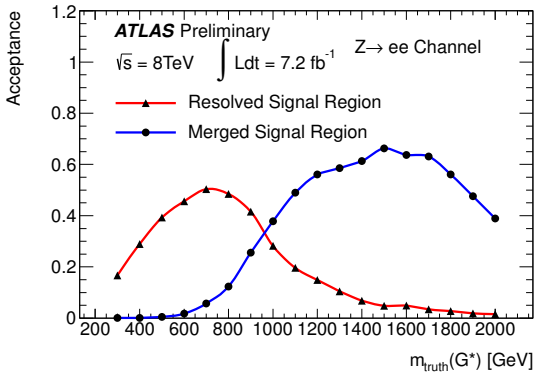

Fig. 5. Signal acceptance for a $G^* \to ZZ$ signal as a function of generated G^* mass for the electron channel. Triangle and solid points show the resolved and merged selections, respectively [14].

The background is estimated by fitting ZZ mass distribution. The fitting function is the same as the dijet analysis (Eq. (1)), where $x = m_{lljj}/\sqrt{s}$ or $m_{llj}/\sqrt{s}$.

Figures 6 (a) and 6 (b) show the distributions of reconstructed (a) m_{lljj} and (b) m_{llj} with estimated backgrounds.

[2] The distance between two points in the pseudorapidity-azimuthal angle space is defined as $\Delta R = \sqrt{(\Delta\eta)^2 + (\Delta\phi)^2}$.

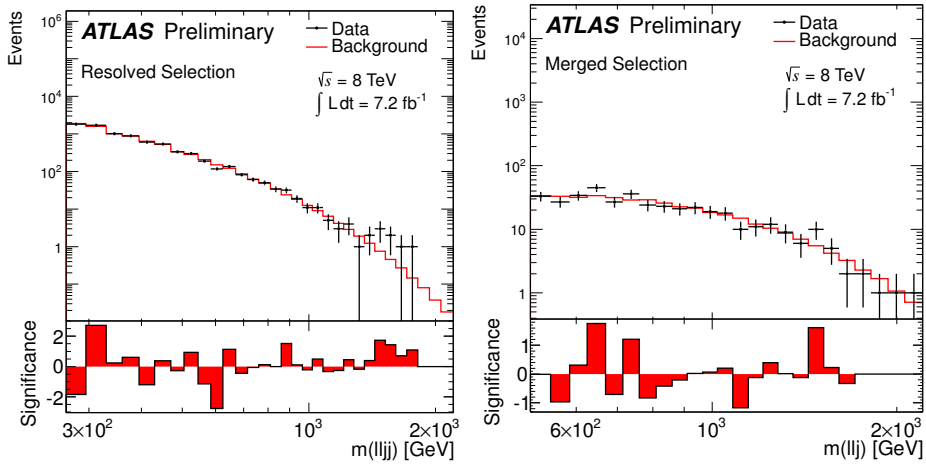

(a) (b)

Fig. 6. Black points with error bars show distribution of reconstructed (a) m_{lljj} and (b) m_{llj}. The lines are estimated backgrounds [14].

A systematic uncertainty from the fitting is less than 5% for m_{lljj} distribution and 10–40% for m_{llj} distribution. The dominant uncertainty of the signal acceptance is the initial state and final state radiations uncertainty, which is evaluated to be 10%. The total uncertainty of signal acceptance is 10–15% depending on the mass.

The result shows the consistency between the data and the estimated background. The 95% C.L. upper limits on $\sigma\,(pp \to G^*) \times \mathrm{B}\,(G^* \to ZZ)$ are evaluated from the result and are shown in figure 7.

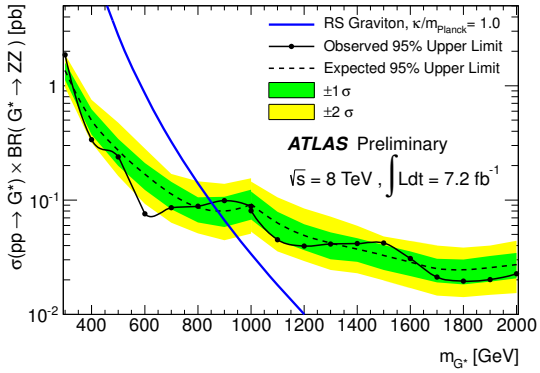

Fig. 7. Observed and expected 95% C.L. upper limits on $\sigma(pp \to G^*) \times \mathrm{B}(G^* \to ZZ)$ for the bulk RS Graviton with a coupling of $\kappa/\bar{m}_{\mathrm{Pl}} = 1$. A solid line represents the leading order theoretical prediction for the bulk RS model [14].

In figure 7, the cross section of the bulk RS Graviton assuming a coupling $\kappa/\bar{m}_{\mathrm{Pl}} = 1$ is also shown[3]. For $\kappa/\bar{m}_{\mathrm{Pl}} = 1$, the observed and expected 95% C.L. lower mass limits of the bulk RS Graviton is 850 and 870 GeV, respectively.

5. Excited lepton search

A search for the excited lepton in the final states of $ll\gamma$ is presented in [17]. This analysis used 8 TeV pp collision data corresponding to an integrated luminosity of 13.0 fb^{-1}.

The analysis searches for events in which the single excited lepton (l^*) is produced associated with a lepton, and decays into a lepton and a photon. The observable used in the analysis is the $ll\gamma$ invariant mass ($m_{ll\gamma}$). The dominant background in this analysis is the Drell–Yan Z/γ^* process. The $Z(\rightarrow ll)+\gamma$ events are the same final states as the signal, and $Z(\rightarrow ll)+$ jets events become background by the jet misidentification as a photon. The latter background is suppressed by the stringent quality requirements for the photon.

Events are selected by requiring two electrons or two muons, and isolated photon. To suppress the Drell–Yan process, $m_{ll} > 110$ GeV is required. Finally, the signal search region for the lower excited lepton mass ($m_{l^*} < 900$ GeV) is defined as $m_{ll\gamma} > m_{l^*} + 150$ GeV. For $m_{l^*} \geq 900$ GeV, the signal search region is $m_{ll\gamma} > 1050$ GeV.

The background estimation is based on the Monte Carlo simulation. The scale factor for Z+jets is estimated from the data in the region $70 < m_{ll} < 110$ GeV. To cover low statistics of the simulated events in the region $m_{ll} > 110$ GeV, Z+jets and $Z+\gamma$ simulation samples are extrapolated from low $m_{ll\gamma}$ region, by fitting the distribution with the exponential function in the range $150 < m_{ll\gamma} < 1050$ GeV.

The uncertainty from the extrapolation is the largest uncertainty in the high m_{l^*} region. It is about 40% for both channels at $m_{l^*} = 2$ TeV, while it is about 6% at $m_{l^*} = 200$ GeV. The theoretical uncertainties of $Z+\gamma$ cross section is evaluated with MCFM [18] and are 6% and 8% for $m_{l^*} = 200$ GeV and $m_{l^*} > 900$ GeV, respectively. Other uncertainties are the luminosity uncertainty of 3.6% and the 4–6% uncertainties from the object reconstructions and triggers efficiencies.

Figures 8 (a) and 8 (b) show distributions of the $m_{ee\gamma}$ and $m_{\mu\mu\gamma}$ after the final selection. The result shows the data is consistent with the estimated background.

[3] κ is the curvature of the wrapped extra dimension. $\bar{m}_{\mathrm{Pl}}$ is the reduced Plank mass.

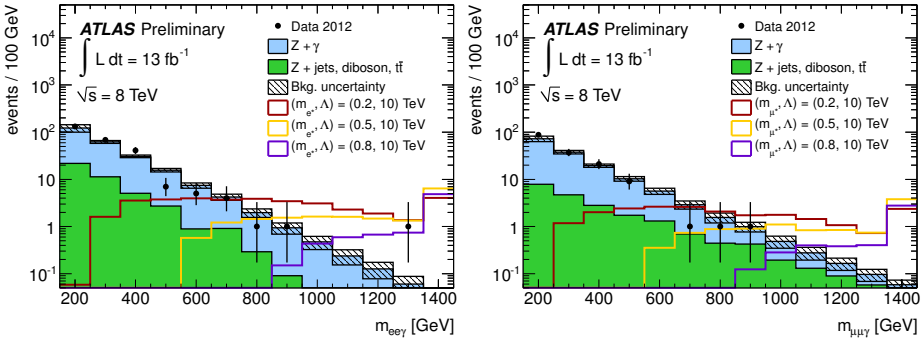

(a) (b)

Fig. 8. Distributions of the (a) $m_{ee\gamma}$ and (b) $m_{\mu\mu\gamma}$ after requiring $m_{ll} > 100$ GeV. Z+jets and $Z + \gamma$ distributions are fitted shape, and uncertainties from the extrapolation are shown as hatched areas. The last bin contains overflow. The signal distributions for different mass with $\Lambda = 10$ TeV are also shown [17].

The evaluated 95% C.L. upper limits on the $\sigma \times B$ for the electron channel is shown in figure 9 (a). The theoretical cross sections for different mass points of signals are also shown. This result is interpreted to the exclusion limits in the $m_{e^*} - \Lambda$ plane, where Λ is the compositness scale, which is shown in figure 9 (b). At $\Lambda = m_{l^*}$, $m_{l^*} > 2.2$ TeV is obtained for both the electron and the muon channels.

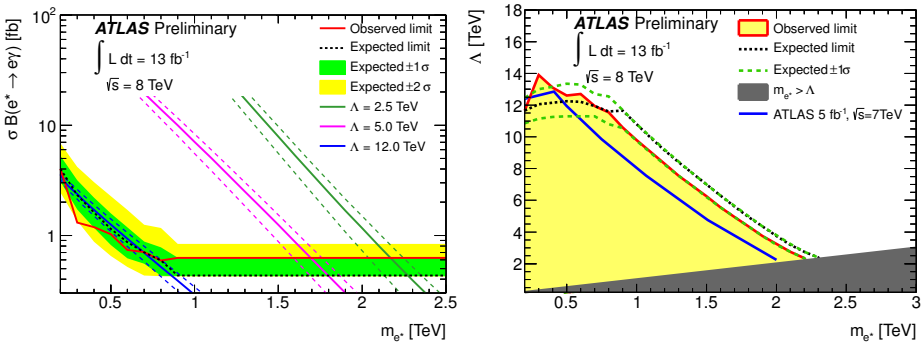

(a) (b)

Fig. 9. (a) The 95% C.L. upper limits on the $\sigma \times B$ as a function of m_{e^*}. (b) Exclusion limits in the $m_{e^*} - \Lambda$ parameter space for e^*. A region to the left of the experimental limit is excluded at 95% C.L. No limits are set in the dark shaded region $m_{e^*} > \Lambda$, where the model is not applicable [17].

6. Mono-jet search

Searched for new phenomena in mono-jet + $E_{\mathrm{T}}^{\mathrm{miss}}$ [4] is reported in [19]. The analysis is performed on data corresponding to an integrated luminosity of 10.5 fb^{-1} of 8 TeV pp collisions. There are some possibilities of mono-jet production such as the graviton emission in ADD model [20] or weakly interacting massive particles (WIMPs) [21], which is a candidate for the Dark Matter.

Events are required to have $E_{\mathrm{T}}^{\mathrm{miss}} > 120$ GeV and the leading jet $p_{\mathrm{T}} > 120$ GeV. Events that have a third leading jet with $p_{\mathrm{T}} > 30$ GeV are rejected. If there is a second jet in an event and it has $p_{\mathrm{T}} > 30$ GeV, it must be separated from $E_{\mathrm{T}}^{\mathrm{miss}}$ as $\Delta\phi\left(\mathrm{jet}, E_{\mathrm{T}}^{\mathrm{miss}}\right) > 0.5$. This requirement removes QCD background events in which miss measurement of the second jet results in large (fake) $E_{\mathrm{T}}^{\mathrm{miss}}$. In addition, no identified electrons or muons are required.

After these event selections, four different signal regions (SR1–SR4) are defined with different leading jet p_{T} and $E_{\mathrm{T}}^{\mathrm{miss}}$ threshold of 120 GeV, 220 GeV, 350 GeV, and 500 GeV.

The dominant background is the Drell–Yan process, in which the Z boson decays into two neutrinos. Other electroweak processes of the Drell–Yan in which the boson decays into charged leptons and W+jets process are also contained. Other physics backgrounds are $t\bar{t}$, QCD multijet and diboson process. Non-collision background induced by the beam and cosmic rays pose additional sources of background.

All electroweak backgrounds are estimated by data-driven method using $W \to \mu\nu$ control sample, which is obtained by requiring one muon, and $40 < E_{\mathrm{T}}^{\mathrm{miss}} < 100$ GeV. For each target electroweak process, the ratio between the target process events in the signal region and $W \to \mu\nu$ in the control region is estimated by using the Monte Carlo simulation. This ratio is calculated bin-by-bin in jet p_{T} distribution. The number of data events is then estimated from the control events in data and this ratio. The total uncertainty for electroweak backgrounds is 4–17% for the SR1–SR4.

QCD background comes mainly from misreconstruction of the jet energy. To estimate this background, the control region is defined by reverting $\Delta\phi\left(\mathrm{jet}, E_{\mathrm{T}}^{\mathrm{miss}}\right)$ cut for single jet background. For two jets, background events are required to have the third jet that has the same condition as the second jet in the single jet control region. The jet p_{T} distributions in these control regions are fitted and extrapolated to the signal region where p_{T} is less than 30 GeV. The systematic uncertainties from this estimation are about 100%. The QCD background is about 1% in the SR1 and SR2, while it is negligible in the SR3 and SR4.

[4] The missing transverse momentum, $E_{\mathrm{T}}^{\mathrm{miss}}$, is the energy imbalance in the transverse plane.

The non-collision background is also estimated by data-driven method, in which the control sample is obtained from the wrong jet timing events, in which a jet generation timing is significantly different from the collision timing. This background is less than 1% in the total background in the signal regions.

Figure 10 (a) shows the leading jet p_{T} distributions in the SR1. The observed data shows good agreement with the background expectation. Figure 10 (b) is the model independent 95% C.L. limits on the cross section times acceptance ($\mathcal{A}$) times efficiency (ϵ) for each signal region. The luminosity uncertainty of 3.6% is considered in the calculation.

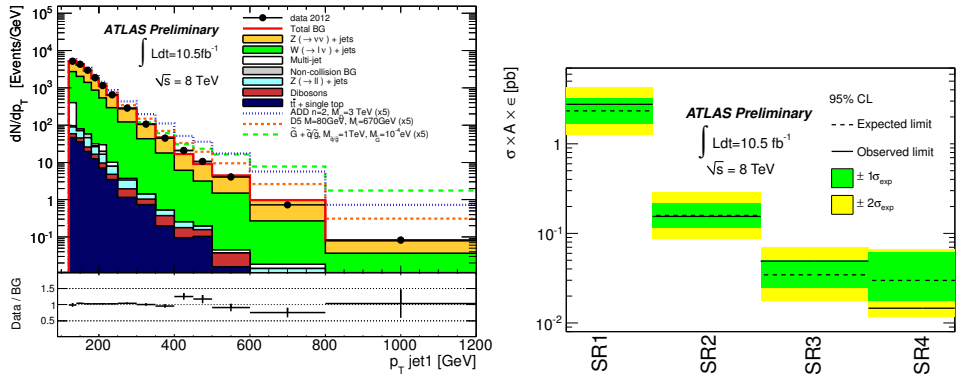

(a) (b)

Fig. 10. (a) The leading jet p_{T} distributions in the SR1. Black dots show the data, filled histograms estimated backgrounds. Some different signal predictions are shown in the dot lines. Only statistical uncertainty is shown in this plot. (b) The model independent observed (solid lines) and expected (dashed lines) 95% C.L. limits on $\sigma \times \mathcal{A} \times \epsilon$ for different signal regions [19].

The interpretation of this result to the ADD model is shown in Fig. 11 (a). The signal prediction uncertainties are 27–50% depending on the parameters. Obtained lower limits on the fundamental Planck Scale (M_{D}) in the ADD model are $M_{\mathrm{D}} > 3.88, 3.16, 2.84, 2.65$, and 2.58 TeV for the numbers of extra dimensions equal to 2, 3, 4, 5, and 6, respectively. Another interpretation is for WIMP production. Figure 11 (b) shows the 90% C.L. lower limits on the suppression mass scale M_* as a function of WIMP mass (m_χ) for vector type vertex operator (D5) case [19]. For D5, the signal prediction uncertainties are 7% for $m_\chi = 80$ GeV, and 88% for $m_\chi \leq 1000$ GeV. Obtained limits are $M_* > 731, 632, 349$ GeV for $m_\chi \leq 80, = 400$, and 1000 GeV, respectively.

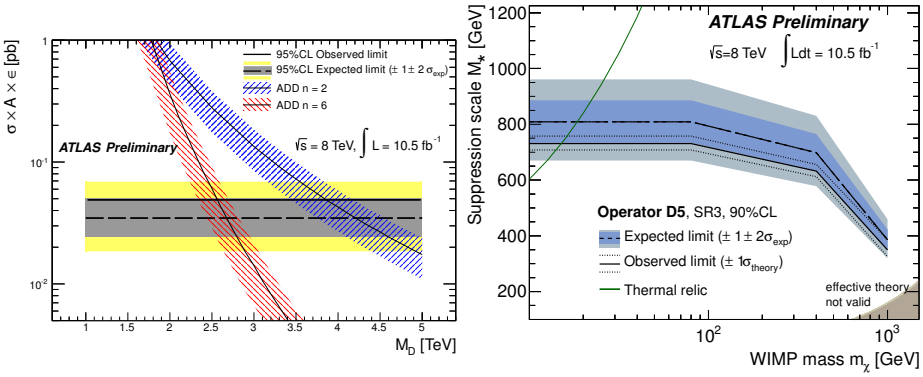

(a) (b)

Fig. 11. (a) The predicted ADD $\sigma \times \mathcal{A} \times \epsilon$ for the SR3 as a function of M_{D} for $n = 2$ and $n = 6$. (b) The 90% C.L. lower limits on M_* as a function of m_χ for vector type vertex operator (D5) case [19].

7. Conclusion

Five searches using 8 TeV *pp* collision data in 2012 have been presented to introduce recent exotics studies in the ATLAS experiment. In summary, no significant deviation from the Standard Model description has been observed in these analyses and limits are set on several Beyond Standard Model scenarios.

New results on searches of Beyond Standard Model physics based on 7 TeV *pp* collision data and on 8 TeV data using the full 2012 data set are being prepared for publication, and will become available soon.

All results of exotics searches in the ATLAS experiment are listed in [22].

REFERENCES

[1] L. Evans, P. Bryant (eds.), *JINST* **3**, S08001 (2008).
[2] D.V. Volkov, V.P. Akulov, *Phys. Lett.* **B46**, 109 (1973).
[3] J. Wess, B. Zumino, *Nucl. Phys.* **B70**, 39 (1974).
[4] S.P. Martin, `arXiv:hep-ph/9709356`.
[5] ATLAS Collaboration, *JINST* **3**, S08003 (2008).
[6] ATLAS Collaboration, ATLAS-CONF-2012-148, `https://cds.cern.ch/record/1493487`
[7] G. Choudalakis, `arXiv:1101.0390 [physics.data-an]`.
[8] L. Lyons, *Ann. Appl. Stat.* **2**, 887 (2008).

[9] ATLAS Collaboration, *J. High Energy Phys.* **1301**, 029 (2013) [arXiv:1210.1718 [hep-ex]].

[10] P. Langacker, *Rev. Mod. Phys.* **81**, 1199 (2009) [arXiv:0801.1345 [hep-ph]].

[11] ATLAS Collaboration, ATLAS-CONF-2012-129, https://cds.cern.ch/record/1477926

[12] ATLAS Collaboration, *Phys. Lett.* **B700**, 163 (2011) [arXiv:1103.6218 [hep-ex]].

[13] D. London, J.L. Rosner, *Phys. Rev.* **D34**, 1530 (1986).

[14] ATLAS Collaboration, ATLAS-CONF-2012-150, https://cds.cern.ch/record/1493489

[15] K. Agashe, H. Davoudiasl, G. Perez, A. Soni, *Phys. Rev.* **D76**, 036006 (2007) [arXiv:hep-ph/0701186].

[16] L. Randall, R. Sundrum, *Phys. Rev. Lett.* **83**, 3370 (1999) [arXiv:hep-ph/9905221].

[17] ATLAS Collaboration, ATLAS-CONF-2012-146, https://cds.cern.ch/record/1493485

[18] J.M. Campbell, R.K. Ellis, *Phys. Rev.* **D60**, 113006 (1999) [arXiv:hep-ph/9905386].

[19] ATLAS Collaboration, ATLAS-CONF-2012-147, https://cds.cern.ch/record/1493486

[20] N. Arkani-Hamed, S. Dimopoulos, G.R. Dvali, *Phys. Lett.* **B429**, 263 (1998) [arXiv:hep-ph/9803315].

[21] G. Bertone, D. Hooper, J. Silk, *Phys. Rep.* **405**, 279 (2005) [arXiv:hep-ph/0404175].

[22] https://twiki.cern.ch/twiki/bin/view/AtlasPublic/ExoticsPublicResults